Accurate determination of dielectronic recombination resonances with lithiumlike argon

W. Zong, R. Schuch, E. Lindroth, H. Gao, D. R. DeWitt, and S. Asp
Department of Atomic Physics, Stockholm University, S-104 05 Stockholm, Sweden

H. Danared
Manne Siegbahn Laboratory, S-104 05 Stockholm, Sweden

(Received 17 January 1997)

A highly accurate measurement of $\Delta n=0$ dielectronic recombination (DR) resonances with Ar^{15+} has been carried out at the ion storage ring CRYRING. The absolute energies of the DR resonances were determined by a method that uses the Schottky frequency and the knowledge of the length of the beam orbit in the ring. The accuracy in the absolute energy achieved in this experiment was $\sim 1\%$. Positions and widths of doubly excited states of Ar^{14+}, as well as the DR cross sections, were calculated with relativistic many-body perturbation theory in an all-order formulation. Radiative corrections and mass polarization were needed to obtain good agreement with the experimental results. [S1050-2947(97)08906-3]

PACS number(s): 34.80.Lx, 31.15.Ar, 31.30.Jv

I. INTRODUCTION

In electron-ion collisions, a free electron may be captured by an ion having bound electrons under simultaneous excitation. This inverse Auger process creates a doubly excited state. If the intermediate state decays radiatively, dielectronic recombination (DR) is completed. DR is a fundamental recombination process. In addition to its application in astrophysics and fusion plasmas [1–3], it is important for studies of the structure and decay channels of atomic doubly excited states. For such studies it is essential that the energy resolution is sufficiently high so that resonances due to different doubly excited states are resolved. Doubly excited states are highly correlated systems which in general cannot be well described without an accurate treatment of electron correlation. If measurements of these states are to provide a stringent test of methods to treat correlation, a high precision in the absolute determination of the energy positions is crucial.

Storage rings with electron-cooling devices provide unique instruments for studies of the DR process. By adiabatic expansion of the electron beam, an ultracold beam is obtained [4], which is the key feature to obtain high resolution. However, in order to determine the absolute resonance energy, a knowledge of the laboratory energy of the electron beam is needed. This information can be obtained from the electron acceleration potential, albeit a careful correction for space-charge effects is required. The space charge of the electron beam may be partially screened by the positive ions that are formed by ionization of the residual gas atoms, and subsequently trapped in the interaction region by the space-charge potential. Usually this effect is included by simply assuming that the contribution from the positive ions is proportional to the electron density. In reality the effects due to the space charge are more complicated, and the systematic error from the inability to correct for it properly accounts for the major part of the uncertainty in the absolute determination of the resonance energies. To overcome this problem, an alternative calibration method was suggested [5]. The idea is to choose the maxima of several resonance peaks of a DR spectrum as calibration points and determine their energies from the measurement of the Schottky frequency and the knowledge of the length of the beam orbit in the ring. The energy values of these maxima are then used to calibrate the energy scale for the whole DR spectrum. The important advantage of this method is that corrections for the space charge and other effects are no longer needed.

Lithiumlike systems are well suited for a comparison of *ab initio* calculations with experimental studies of the DR process due to the relatively simple structure of both the Li-like initial ion and the Be-like recombined ion which makes them within reach of an accurate theoretical treatment. In earlier measurements of $\Delta n=0$ DR of Ar^{15+} [6], the resolution was in the eV region due to a rather high temperature of the electron beam and the use of a single-pass technique. Here we present a DR measurement for the same system with nearly two orders of magnitude improvement of the resolution as well as of the absolute energy accuracy. The better accuracy is due not only to the use of an expanded electron beam in a storage ring but also due to a calibration method which allows a determination of the resonance positions with a precision of around 10 meV.

In a recent article by Gorczyca *et al.* [7], several calculations schemes were compared for the case of Ar^{15+}, the agreement with Ref. [6] is good in all cases. When compared to the present measurement, however, there are differences between the calculated and measured energy positions which are clearly outside the experimental error bars [8]. The differences fluctuate, and cannot be accounted for by a simple shift of the theoretical spectrum. The differences also increase with decreasing ℓ values of the outermost electron in the recombined ion. That the agreement with the more accurate experiment is not perfect is not surprising, since these calculation schemes treat correlation and relativistic effects in low order, and do not consider radiative corrections. To match the experimental accuracy, a more careful theoretical treatment is necessary.

Here we compare the experimental data with the result of a fully relativistic calculation which also accounts for correlation to high orders. The contributions to the energy positions from QED corrections as well as from the Breit inter-

action are 100–200 meV. Correlation contributions from the inner electrons ($1s^2 2\ell$) are of the same size, and for the low-energy DR resonances even the detailed interaction between the outer electron (with $n \geqslant 10$) and the inner electrons reaches the size of nearly 100 meV in some cases. The agreement between theory and experiment for the energy positions is, with the exception of one resonance, within the experimental error bars. For the rate coefficient, the agreement is within 15%, and thus also within the experimental error bars. The experimental method is described in Sec. II, and the theoretical treatment in Sec. III. The results are discussed in Sec. IV.

II. EXPERIMENT

A. Measurement

The experiment was carried out with CRYRING at the Manne Siegbahn Laboratory [9] in Stockholm. The Ar^{15+} beam was produced in an electron beam ion source (CRYSIS), and injected into the ring after preacceleration by a radio-frequency quadrupole accelerator to the injection energy of 300 keV/amu. Acceleration of the circulating ion beam to the designed energy was done by a radio frequency driven drift tube [10]. The average number of ions stored in the ring was determined to be 1.3×10^5, from measurements of the ion beam current using a beam current transformer. The uncertainty in the ion number determination was $\sim$30%. The ion and electron beam currents were 0.3μA and 96 mA, respectively. The recombined Ar^{14+} ions were separated from the circulating beam by the first dipole magnet after the cooler and detected by a surface barrier detector (SBD).

We started the DR measurement at the ion energy of 11 MeV/amu by scanning the electron energy over a range which covered all $\Delta n=0$ DR resonances. The scan started after cooling of the ion beam for 3 s. The cathode voltage went first up, then down from its maximum, crossing the cooling voltage to the minimum and back to the cooling voltage again. The total time of this sawtooth voltage scan was 4 s and the scan covered the energy region of approximately 0–40 eV in the center of mass (c.m.) frame four times, twice when the electron velocity was higher than the ion velocity, and twice when the electron velocity was lower than the ion velocity. After each injection of a new ion beam the cycle started again. The data were taken in 1720 complete cycles. Each recorded event consisted of the SBD pulse height, the cathode voltage, and a time ramp digitized in 3000 steps. More details of this scanning method can be found in Ref. [11]. The data recorded contained four complete DR spectra. They were then, after transformation to the c.m. frame, calibrated by our method.

The calibration method can be explained briefly as follows. For each of the calibration points (usually the maxima of the prominent resonance peaks) chosen in the DR spectrum, the corresponding cathode voltage of the cooler is first recorded. The cathode voltage is then set to each recorded value, and the ion energy is adjusted until new cooling is reached. Under cooling condition, the velocity of the electron beam matches the velocity of the ion beam, that is $v_e=v_i$, where v_e and v_i denote the electron velocity and ion velocity at cooling, respectively. Since the latter can be derived from the Schottky frequency f_s by $v_i=f_sL$, where L is the length of the stored beam closed orbit, the velocity and the energy of the electrons can be readily deduced. It should be pointed out that the electron energy deduced in this approach is the absolute one; the effect of the space charge is automatically included, and need not be corrected for.

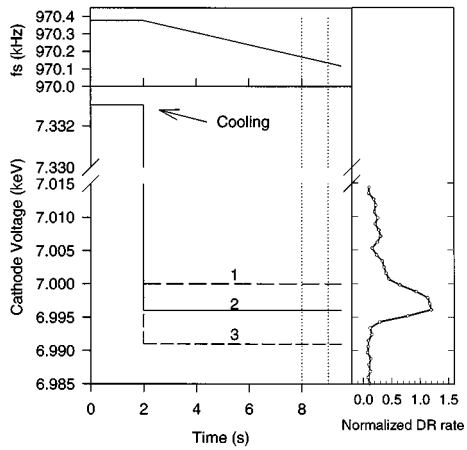

FIG. 1. The main part schematically shows the cathode voltage as a function of time. The lines numbered 1, 2, and 3 indicate three scan steps. For each step, the recombination rate was recorded in the time window indicated by the dotted vertical lines. As the ion energy shifts due to the drag force, the changing Schottky frequency (shown schematically in the upper part of the figure) was measured in the same time window. The normalized rate spectrum obtained by the scan is displayed in the right part of the figure. The cathode voltage where the rate has a maximum is taken as the calibration point.

In more detail, the absolute energy measurement of the calibration points was performed here in the following steps.

(i) The maxima of the five highest resonance peaks in the region of interest were chosen as calibration points. Those points were well defined and close to the relevant DR resonances.

(ii) The cathode voltage for each chosen calibration point has to be precisely determined. However, this cannot be done by a smooth voltage scan over the calibration point because of a time delay in the response of the power supply feeding. Instead, the cathode voltage was set to a certain value by a sharp drop from cooling in each scan step. The recombination rate was recorded both at cooling and at the set cathode voltage. The value for the cathode voltage at the calibration point should be taken as that where the DR rate has a local maximum. Two factors that may affect the DR rate were taken into account in order to find the true maximum. First, since the rate is proportional to the ion beam intensity, which may fluctuate at different scan steps, the rate at cooling was used to normalize the DR rate recorded at the scan step. Second, since the ion energy changed while the cathode voltage was at the set cathode voltage due to the drag force, a time window was set to ensure that the DR rate was recorded at the same and well-known ion energy in all scan steps. Also the Schottky frequency (f_{s1}) was measured in the same time window so that it reflected the ion velocity when the cathode voltage was at the calibration point. Figure 1 shows schematically the method used to determine the cathode volt-

age for one of the calibration points.

(iii) The cathode voltage of the cooler was set to the obtained values successively. At each energy value, the ion energy was adjusted until cooling was reached once more, and then the Schottky frequency was measured again. As the electron velocity matches the ion velocity under cooling, this Schottky frequency (f_{s2}), reveals the electron velocity at the calibration point.

With this procedure a pair of Schottky frequencies (f_{s1} and f_{s2}) were obtained for each calibration point. The ion and electron energies at each point were then derived from the Schottky frequencies f_{s1} and f_{s2}, respectively. This procedure was repeated for each chosen calibration point. As pointed out above, the electron energies obtained are the *real* energies which include all corrections. They can be used directly in the transformation from the laboratory frame to the c.m. frame.

B. Data analysis and error estimation

The calculation of the relative velocity v_r and the c.m. energy E for each calibration point is rather straightforward,

$$v_r=\frac{(f_{s1}-f_{s2})L}{1-f_{s1}f_{s2}L^2/c^2}, \quad E=\left(\frac{1}{\sqrt{1-(v_r/c)^2}}-1\right)\mu c^2, \tag{1}$$

where f_{s1} and f_{s2} constitute the measured Schottky frequency pair, and $\mu=m_e m_i/(m_e+m_i)$ is the reduced mass. L is the orbit length of the ion beam in the ring, and is estimated from

$$L=L_0+2\pi r_{\text{shift}}, \tag{2}$$

where L_0 stands for the length of the nominal closed orbit of the ion beam, and r_{shift} is the offset of the beam from this closed orbit. In this measurement a beam offset was necessary because of the small separation between the circulating beam (Ar^{15+}) and the recombined beam (Ar^{14+}). If the detector had been placed where Ar^{14+} could be detected, the circulating Ar^{15+} beam would be blocked because of the large beam size before cooling. The detector was therefore positioned at a place where it did not block the ion beam, allowing it to be cooled in the nominal closed orbit. Once cooled and shrunk in size, the ion beam was shifted to a larger orbit by r_{shift}, so that the recombined ions could be detected. The distance r_{shift} was 1.5 ± 0.3 cm. It was measured by probing the beam position before and after the shift of the ion beam. The obtained value was checked by the estimated space-charge potential difference between the two positions. The error in r_{shift} corresponds to an error of about 2 cm in L, and was added to the uncertainty, of around 4 cm [12], caused by using the ring length along its axis (5163 cm) as the length of the nominal orbit L_0. The total uncertainty of L was thus estimated to be $\Delta L\approx 6$ cm.

The measured Schottky peaks were around 9 MHz, with a width of approximately 300 Hz. We used $\sigma=125$ Hz for an estimate of the uncertainty in the frequency determination. This might be an overestimate, but it does not affect the ultimate accuracy very much due to its small contribution to the total uncertainty. The uncertainty of the ground Schottky frequencies were estimated to be $\Delta f_s=12$ Hz from the fact that the measured Schottky frequencies were the tenth harmonic.

TABLE I. Experimental energies and estimated errors of the calibration points. The E_c's are the energies of the five calibration points derived from the Schottky frequency measurement. They are used in the calibration of the DR spectrum. ΔE_c is the total uncertainty in E_c measurements. The total uncertainty (ΔE_{total}) is the sum of the ΔE_c and the uncertainty in determination of the maxima energy, $\Delta E_{\max}$.

Calibration points	1	2	3	4	5
E_c (eV)	1.217	4.365	6.503	9.613	13.644
ΔE_{fs1} (eV)	0.0024	0.0045	0.0054	0.0066	0.0079
ΔE_{fs2} (eV)	0.0089	0.0167	0.0204	0.0248	0.0296
ΔE_L (eV)	0.0030	0.0107	0.0159	0.0234	0.0335
ΔE_c (eV)	0.0097	0.0203	0.0264	0.0347	0.0453
$\Delta E_{\max}$ (eV)	0.0052	0.010	0.012	0.015	0.018
ΔE_{total} (eV)	0.015	0.030	0.038	0.050	0.063
$\Delta E_{\text{total}}/E_c$	1.2 %	0.69%	0.59%	0.52%	0.46%

Because of the difficulty to bring the ion beam precisely back to its original position for new cooling after the change of the cathode voltage, the Schottky frequencies f_{s2} were measured by an indirect method. Instead of trying to put the beam back precisely, we moved the beam to some position close to the original one and recorded the Schottky frequencies as a function of the beam position. An interpolation was then used to derive the Schottky frequency corresponding to the original beam position, which is needed by Eq. (1), used in the transformation to the c.m. frame. The uncertainty in the Schottky frequency f_{s2} caused by this approach was estimated as follows: An uncertainty of 1.0 mm in the beam position corresponds to an uncertainty of approximately 38 Hz in the Schottky frequency in the interpolation. The total uncertainty of the Schottky frequency f_{s2} is thus estimated as $\Delta f_{s2}=\sqrt{(45)^2+(12)^2}$ Hz$\approx$46 Hz, where 45 Hz is the frequency uncertainty corresponding to the uncertainty of 1.2 mm in the beam position determination. The derived absolute energies and the error caused by the uncertainties in L and f_{s1}, f_{s2} are listed in Table I.

For the calibration of the whole DR spectra, it was first transformed to the c.m. frame by a procedure similar to that used in our previous DR experiments [11], and the calibration points were then aligned to the corresponding energy values calculated from the Schottky frequency pairs. Another error which has been considered is that the true local maxima in the DR spectrum might lie between scan steps. This causes an error in the energy calibration because the calibration points are then not aligned with correct points in the spectrum. Since the scan was performed only once for each peak, this error was estimated to be half of the energy bin size of the scan step. This error is converted into c.m. energies and listed together with the other errors in Table I.

TABLE II. The contributions to the splittings between the $1s^2 2s_{1/2}$, $1s^2 2p_{1/2}$, and $1s^2 2p_{3/2}$ states in Ar^{15+}.

	$2p_{1/2}$-$2s_{1/2}$ (eV)	$2p_{3/2}$-$2s_{1/2}$ (eV)	$2p_{3/2}$-$2p_{1/2}$ (eV)
Dirac-Fock	32.017	35.349	3.332
Δ Dirac-Fock-Breit	0.152	-0.026	-0.178
Retardation beyond Breit	0.000	-0.002	-0.001
Coulomb correlation	-0.164	-0.155	0.009
Breit correlation	0.002	0.003	0.001
Radiative corrections [a]	-0.130	-0.122	0.008
Mass polarization	-0.008	-0.008	0.000
Total	31.868	35.040	3.171
Present experiment			3.16 ±0.02
Experiment [b]	31.866±0.001	35.037±0.001	3.171±0.001

[a]Screened self-energy and vacuum polarization, Blundell 1993, Ref. [16].
[b]Astrophysical observation by Widing and Purcell 1976, Ref. [17].

In order to determine resonance strengths from the spectra, the counts of the DR spectra were converted to rate coefficients by the formula

$$\alpha(E_c) = \frac{N_c \gamma^2}{N_{\mathrm{cyc}} \delta t N_i n_e l / L}, \tag{3}$$

where the E_c is the energy corresponding to channel c and N_c the number of counts in that channel. N_{cyc} is the number of measuring cycles, and δt is the time interval per channel. The Lorentz factor is denoted by γ, $n_e(E_c)$ stands for the electron density at the energy E_c, N_i is the number of ions stored, and l is the interaction length. The uncertainty of the rate coefficient was estimated to be 30%, determined mainly by the uncertainty in N_i.

III. THEORETICAL TREATMENT

In the calculation we consider electrons recombining with Ar^{15+} into doubly excited states of Ar^{14+}, which then decay radiatively to states below the ionization threshold. There are two main channels

$$Ar^{15+}(1s^2 2s) + e^- \rightarrow Ar^{14+}(1s^2 2p_j n \ell j') \tag{4}$$

$$\rightarrow Ar^{14+}(1s^2 2s n \ell j'') + h\nu \tag{5}$$

and

$$\rightarrow Ar^{14+}(1s^2 2p_j n' \ell' j''') + h\nu, \tag{6}$$

where n' should be low enough that the recombined ion is below the ionization limit. The latter channel is by far the most important, being 10–100 times stronger than the first channel for all the calculated doubly excited states. This dominance of the latter channel was also found in a recent study by Gorczyca *et al.* [7]. The DR resonances are found for electron energies

$$\varepsilon_{e^-} = E(Ar^{14+}{}^{**}(1s^2 2p_j n \ell j')) - E(Ar^{15+}(1s^2 2s)). \tag{7}$$

TABLE III. A breakdown of the contributions involving the outer electron to the positions of the Ar^{14+} $2p_{1/2}10p_j$ resonances.

	$2p_{1/2}10p_{1/2}$ (eV)		$2p_{1/2}10p_{3/2}$ (eV)	
$(2p_{1/2}$-$2s_{1/2})$ [a] +				
Dirac-Fock description of $10p_j$	0.922		0.933	
Δ Dirac-Fock-Breit for $10p_j$	0.014		0.021	
polarization of $1s^2$ by $10p_j$	-0.001		-0.001	
	$J=0$	$J=1$	$J=1$	$J=2$
$2p_{1/2}10p_j$ correlation	0.093	-0.036	0.012	0.025
Total	1.028	0.898	0.965	0.977

[a]The $2p_{1/2}$-$2s_{1/2}$ splitting includes correlation and relativistic effects as listed in Table II.

Since, in Ar^{15+}, the splitting is 33.87 between the $1s^2 2s_{1/2}$ and $1s^2 2p_{1/2}$ states and 35.04 eV between the $1s^2 2s_{1/2}$ and $1s^2 2p_{3/2}$ states, the first resonances are readily estimated to appear for $n=10$. As can be seen from Table II, a careful inclusion of correlation as well as of relativistic and radiative effects is necessary to reproduce these splittings.

Our calculation is done with a method which combines relativistic many-body perturbation theory in an all-order formulation, described for three- and four-electron ions in Ref. [13], with complex rotation. Complex rotation is employed in order to deal with autoionizing states, and the calculation directly gives the widths together with the energy positions. The combination with many-body perturbation theory is, for the nonrelativistic case, described in Ref. [14,15].

For the inner electrons ($n=1$ and 2) correlation is included due to the Coulomb as well as Breit interactions. The most important radiative effects, self-energy and vacuum polarization, have been calculated for lithiumlike systems with a high accuracy by Blundell [16], and his results have been added to our calculation; the sizes of the different contributions are shown in Table II. The outer $n=10$ electron is first described as moving in the Dirac-Fock-Breit potential from the $1s^2$ core, and a spherical symmetric potential accounting for the main screening effects from the inner $2p$ electron. The polarization of the closed $1s^2$ core by the outer electron is included, although it is a small contribution when the latter is in such a high-n state like $n=10$. A breakdown of the contributions involving the outer electron is shown for a few resonances in Table III. Radiative effects scale as $1/n^3$ and are thus less important for high-n states. Finally the detailed Coulomb interaction between the outer electron and the $2p$ electron is considered. This contribution is quite different for states coupled to different total J, as can be seen on the fourth line of Table III. For some of the $n=10$ and low-ℓ configurations, the different total J states are separated enough that they can be distinguished in the experimental spectrum, see Fig. 2.

The integrated cross section, or resonance strength S_d, can be written as

$$S_d = \frac{\hbar\pi^2}{k^2}\frac{g_d}{g_i}\frac{A^a_{i\to d}\sum_s A^{\rm rad}_{d\to s}}{A^a_{i\to d}+\sum_s A^{\rm rad}_{d\to s}}, \tag{8}$$

where the multiplicity of the intermediate doubly excited state is given by g_d and that of the initial target state by g_i; here $g_i=2$, and $k=p/\hbar$ is the electron wave number. $A^a_{i\to d}$ is the transition rate into the doubly excited state d. Here this rate equals the autoionization rate from the doubly excited state in the time-reversed process. The rate is obtained from the autoionization width as $A^a=\Gamma/\hbar$. $A^{\rm rad}_{d\to s}$ is the radiative transition rate from state d to a state s, below the ionization threshold. For the doubly excited states ($1s^2 2p10\ell$) with a low ℓ value, up to $\ell=f$ at least, we have $A_a \gg A_r$ and the resonance strength is completely dominated by the radiative rate. This applies then to all resolved resonances in the experimental data. However, for the highest ℓ values some J symmetries show a clear deviation from this rule. The radiative rate dominates in these cases over the autoionization rate, and the magnitude of the rate coefficients close to the series limit decreases accordingly. The rates $A^{\rm rad}$ are calculated within the dipole approximation, and we have only considered one-photon–one-electron transitions. The only approximation which is of any importance is the neglect of two-electron transitions, which gives an uncertainty in the resonance strengths of 10–20 %. This is, however, in the same order of uncertainty with which the rate coefficients can be absolutely determined experimentally. Table IV shows calculated positions, widths, and resonance strengths for a few of the resonances due to the $(1s^2 2p_{1/2}10\ell_j)_J$ states. The resonance strengths from all resonances, 38 from the $2p_{1/2}10\ell_j$ and 72 from the $2p_{3/2}10\ell_j$, were folded with the electron beam temperatures to obtain the theoretical curves as discussed in Sec. IV.

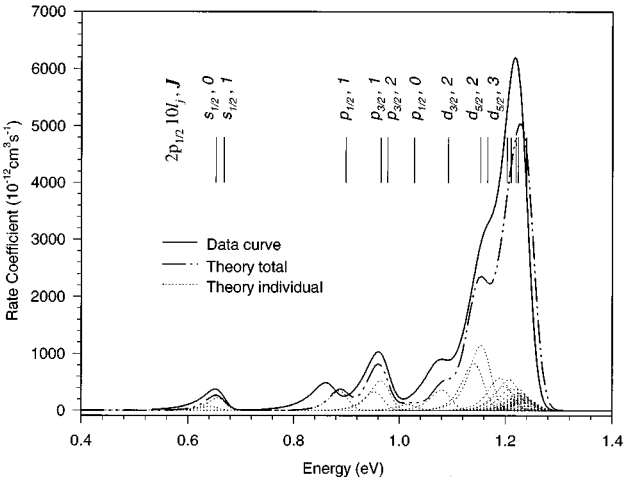

FIG. 2. Contributions from individual DR resonances to the total $1s^2 2p_{1/2}10\ell$ resonance peak. The calculated strengths of the 38 resonances were folded with the temperatures $kT_\perp=20$ meV and $kT_\parallel=0.13$ meV and displayed individually by thin dotted lines. The energy positions of the calculated resonances are indicated in the figure. Due to the difference in $T_\perp$ and $T_\parallel$, the resonance peaks have an asymmetric shape and the resonance energies are situated above the maximum of each peak. The dot-dashed line is the sum of the 38 DR resonances and the solid line is the data represented by a fit curve.

IV. RESULTS AND DISCUSSION

In Table I, the absolute energies of the five calibration points (maxima of the resonance peaks) E_c are listed. The errors due to the uncertainties in the length of the beam orbit (ΔE_L), the Schottky measurements (ΔE_{fs1},ΔE_{fs2}), and the maxima determination ($\Delta E_{\rm max}$), are listed individually to show their contribution to the total uncertainty. As shown by the table, an accuracy of $\sim 1\%$ has been achieved. The absolute energy uncertainty in the present measurement was mainly caused by the offset of the ion beam from its nominal orbit, which resulted in an extra uncertainty in the orbit length and a larger error in the fs_2 measurement. The uncertainty in the fs_2, despite still being apparently small ($\Delta fs_2/fs_2 \sim 10^{-5}$), accounts for the major error in the energy determination, especially when the energy of the calibration point is low, because it is the frequency difference $\Delta(fs_2-fs_1)/(fs_2-fs_1)$ that determines the energy accuracy. In the higher-energy region, the uncertainty in the beam

TABLE IV. Comparison between theory and experiment for the positions of a few of the resonances due to doubly excited states in Ar^{14+}. The calculated autoionization width and strength of the resonances are also listed. The experimental positions are obtained from a fit of the peaks in the spectrum to flattened Maxwellian line profiles. The error bars show the goodness of the fit. In Sec. II it is discussed how the identification of calculated resonance positions with peak positions obtained from the fit is done.

		Resonance position (eV)		Width (eV)	Strength (10^{-20} cm^2 eV)
		Theory	Experiment	Theory	Theory
$2p_{1/2}10s_{1/2}$	$J=0$	0.652		0.002	6.4
	$J=1$	0.667	0.666±0.007	0.009	20.7
$2p_{1/2}10p_{1/2}$	$J=0$	1.028		0.014	8.9
	$J=1$	0.898	0.874±0.016	0.002	29.9
$2p_{1/2}10p_{3/2}$	$J=1$	0.965		0.007	28.5
	$J=2$	0.977	0.976±0.011	0.001	45.3
$2p_{1/2}10d_{3/2}$	$J=1$	1.202		0.004	47.7
	$J=2$	1.092	1.086±0.011	0.000	30.5
$2p_{1/2}10d_{5/2}$	$J=2$	1.153		0.004	70.1
	$J=3$	1.166	1.170±0.010	0.002	95.7

orbit length becomes more important and may ultimately limit the achievable accuracy. The accuracy could be improved if the offset of the beam from the nominal closed orbit was not necessary. Then all measurements could be made with the ion beam in the optimal orbit, obtained by minimizing the Schottky frequency. Another major uncertainty comes from the determination of the cathode voltage of the maxima, which may be improved by making several fine voltage scans to reduce the statistical error.

A. High-energy resonances and series limits

Figure 3 shows the calibrated DR spectrum corresponding to the first part of the energy scan, from cooling to voltage maximum. Because of the good beam quality after cooling, this data set is of highest quality, and is chosen to represent the experimental result. The other three data sets are mainly used for consistency checks. As expected, the $1s^2 2p_{1/2} n\ell$ and $1s^2 2p_{3/2} n\ell$ DR resonance series start with $n=10$, and are clearly seen with two separated series limits. The $1s^2 2p_{1/2} n\ell$ and $1s^2 2p_{3/2} n\ell$ pairs, resonances with the same n but belonging to different series, can be identified up to $n=18$. The resonance peaks belonging to the $1s^2 2p_{3/2} n\ell$ series can be identified even further, up to $n=23$, with the help of calculations [8], while the $1s^2 2p_{1/2} n\ell$ series are not visible due to the lower DR rates.

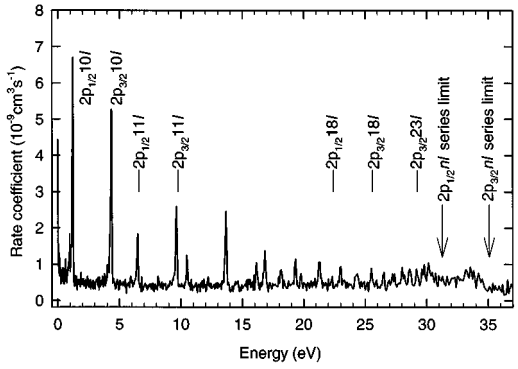

FIG. 3. The calibrated $\Delta n=0$ DR spectrum of Ar^{15+}. The maxima of the left five peaks were aligned to the energies obtained by the Schottky measurement. The spectrum shows clearly the $2p_{1/2} n\ell$ and $2p_{3/2} n\ell$ resonance series. The two bumps at the high-energy side are the two separated series limits. The $2p_{1/2} n\ell$ and $2p_{3/2} n\ell$ pairs which can be well identified are indicated. The first two groups of resonances, from $2p_{1/2}10\ell$ and $2p_{3/2}10\ell$, are displayed in more detail in Fig. 4.

The electron energy at a DR resonance corresponding to a state $1s^2 2p_j n\ell$, with high-n and -ℓ values, can be approximately described by the formula

$$\varepsilon_{e^-} \approx E(1s^2 2p_j) - E(1s^2 2s_{1/2}) - \frac{Z^2}{n^2} \text{ Ry}, \qquad (9)$$

where Z is the charge of the ion core; here $Z=15$, and 1 Ry=13.605 698 eV. These energies can be estimated with an error of less then 10 meV for the highest ℓ values and $n>15$, as there exist a spectroscopic measurement from an astrophysical observation, with an accuracy of 1 meV, for the $1s^2 2p_j n\ell$ - $1s^2 2s_{1/2} n\ell$ splitting [17]. This uncertainty of 10 meV is much smaller than our experimental error in this energy region, which is around 100 meV. As a check of the uncertainty over the whole energy range, our measured energies of the $n=15$–23 resonances were compared with the values predicted by Eq. (9), and all deviations were found to be within the experimental error bars.

For high-n states, the loosely bound electrons may be stripped off by the motional field of the dipole magnet. Only the ions in the states $n<n_{\text{cut}}$, where n_{cut} is the highest n state which is not field ionized, can be detected. Here n_{cut} is estimated to be 43. However, states with $n>n_{\text{cut}}$ have the possibility to decay to states below n_{cut} before entering the dipole magnet, and thus become detectable. This, together with the possible influence of the external field in the interaction region, complicates the analysis of the series limits. We thus did not try to make a detailed analysis of them.

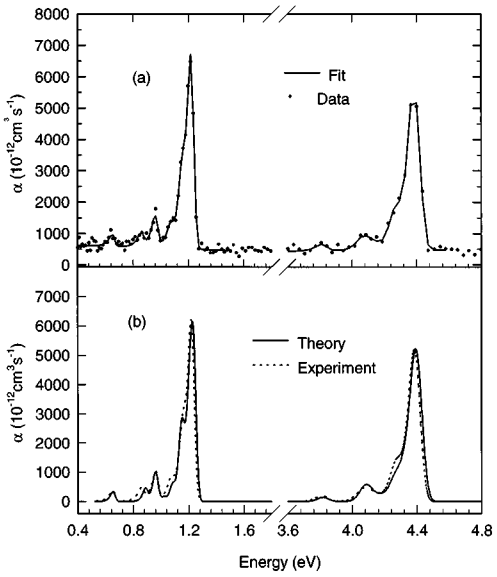

FIG. 4. A detailed DR spectrum of the low energy region which contains the $1s^2 2p_{1/2} 10\ell$ and $1s^2 2p_{3/2} 10\ell$ peaks. The resolution is in the order of 10^{-2} eV FWHM. The fine structure is partly resolved. In (a) the solid lines are obtained from a fit of the data to flattened Maxwellian line profiles. The obtained energy positions for the resonances belonging to $1s^2 2p_{1/2} 10\ell$ are listed in Table IV. (b) Comparison between the measurement and calculation for the $1s^2 2p_{1/2} 10\ell$ and $1s^2 2p_{3/2} 10\ell$ peaks. The experimental curves were generated by a convolution of the fit resonances with the temperatures obtained by the fits. The theoretical curves include all DR resonances involved, 38 and 72, respectively, and are folded with the temperatures $kT_\perp = 20$ meV and $kT_\parallel = 0.13$ meV. The curves were scaled by a factor of 1.2 to match the height of the data curves.

The energy differences between the $1s^2 2p_{1/2} n\ell$ and $1s^2 2p_{3/2} n\ell$ pairs can be derived from the data up to $n = 18$. They should in principle converge to the $1s^2 2p_{1/2} - 1s^2 2p_{3/2}$ fine-structure splitting as $n \to \infty$. However, the values derived from these pairs fluctuate and show no visible tendency. Deriving the energy splitting by extrapolation from them was thus not a reliable method. Instead we used the fact that the most prominent resonances for each $1s^2 2p_{1/2} n\ell$ and $1s^2 2p_{3/2} n\ell$ pair are due to the states with high ℓ. In these states the interactions between the outer $n\ell$ electron and the inner core of $1s^2 2p_{1/2}$ and $1s^2 2p_{3/2}$ differ only to a minor extent. Our theoretical estimate indicates that this difference is already for $n = 10$ and $\ell = 9$, within a few meV and is expected to be smaller for higher $n\ell$. The energy differences between the resonance pairs are thus a good approximation, within 20 meV, for the splitting between $1s^2 2p_{1/2}$ and $1s^2 2p_{3/2}$. The result obtained by a weighted average of the values derived from the $n = 10$–18 pairs is included in Table II. It agrees with the value obtained by the astrophysical observation [17].

B. Low-energy resonances

The parts of the spectrum containing the $1s^2 2p_{1/2} 10\ell$ and $1s^2 2p_{3/2} 10\ell$ pair are displayed in Fig. 4(a). The resonances with different ℓ_j are partially resolved. The energy resolution achieved was in the order of 10^{-2} eV full width at half maximum (FWHM). In order to determine the energy positions of the resonances, fits of the resonance peaks to flattened Maxwellian line profiles were performed. We chose to assign only one resonance line to each of the resolved or partially resolved features of the peaks, since it was not realistic to obtain energy positions for all overlapping resonances. The fit curves are also displayed in the figure to show the quality of the fits. The energy positions of the resonances obtained by the fit to the $2p_{1/2} 10\ell$ peaks are listed in Table IV. The error bars are the standard deviations of the values from fits to the same resonance peaks in the four data sets, see Fig. 5.

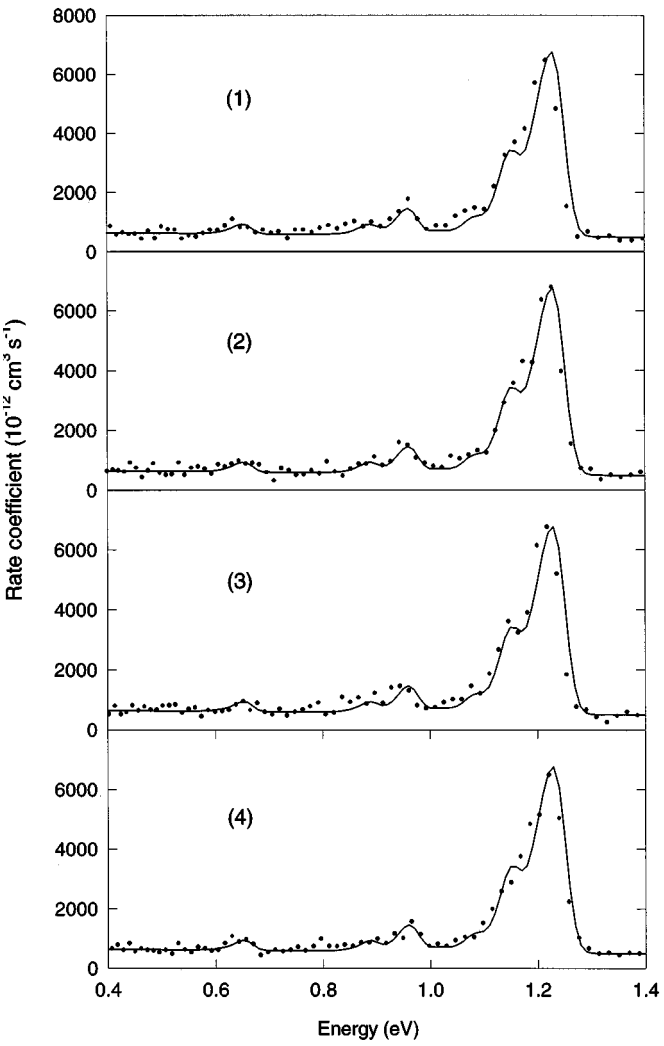

FIG. 5. Comparison of the theory to all four data sets obtained in the present experiment. The four spectra exhibit the same features except around 0.9 eV, where the data show some scattering.

Electron-beam temperatures were checked as free parameters in the fit to the lowest-energy resonances, $1s^2 2p_{1/2} 10\ell$, which yielded a longitudinal temperature of $kT_\parallel = 0.13$ meV and a transverse temperature of $kT_\perp = 30$ meV. While the value of the longitudinal temperature was reasonable, the transverse temperature was higher than expected (around 10 meV). It was also higher than what was obtained in our earlier DR experiment [11], with the same cooler setting. This was probably caused by unresolved resonances. The accumulation of resonances, with slightly differ-

ent energies, might have broadened the shape of the peaks so that the temperature obtained by the fit appeared higher than it actually was. Since the shape of the resonances is determined mainly by the transverse temperature in the low-energy region, only this temperature was affected. With knowledge of the temperatures obtained in other experiments with the same cooler setting, $kT_{\perp}=20$ meV is a reasonable estimate. This is supported by the good agreement between the data and the theoretical curve folded with $kT_{\perp}=20$ meV, displayed in Fig. 4(b), and discussed below.

C. Comparison with the calculation

A comparison of the data with the calculation is shown in Fig. 4(b). In the figure, the data are represented by the fit curves. To obtain the theoretical curves, all 38 resonances in the case of $(1s^2 2p_{1/2} 10\ell_j)_J$ and 72 in the case of $(1s^2 2p_{3/2} 10\ell_j)_J$ were calculated, as discussed in Sec. III, and the theoretical strengths were folded with the electron-beam temperatures $kT_{\perp}=20$ meV and $kT_{\parallel}=0.13$ meV. The experimental rate coefficients are higher than the theoretical values and the theoretical curves were scaled by a factor of 1.2 to match the data curves. The discrepancy in the rate coefficient is within the experimental uncertainty of 30%. The agreement between theory and experiment is in general very good, as shown in the figure. A detailed comparison shows that the theoretical peak at 0.9 eV might be slightly shifted to higher energies compared to the experimental resonance. Although the theoretical position is outside the experimental error bars (see Table IV), it is clear from the four subsequent scans presented in Fig. 5 that the experimental determination of this peak is somewhat uncertain. Another place where the agreement is not perfect is the low-energy side of the large peak, around 1.15 eV, where the calculation indicates some structure which might not be resolved in the experiment. In addition there is a shoulder at the low-energy side of the largest $(1s^2 2p_{1/2} 10\ell)$ peak around 1.04 eV, which is more pronounced in the experimental than in the theoretical curve and there is a similar situation for the largest $(1s^2 2p_{3/2} 10\ell)$ peak. The four subsequent scans in Fig. 5 show, however, that the exact sizes of these shoulders are somewhat uncertain. Finally, the theoretical series limit are slightly higher in energy than the experimental ones, but this difference is clearly within the uncertainty in the absolute energy determination.

To reveal the origin of the resonances found in the experimental data, the calculated resonances of the $(1s^2 2p_{1/2} 10\ell_j)_J$ states were folded individually and displayed as dashed lines in Fig. 2. It is clear that the stronger $J=1$ resonance in the $(1s^2 2p_{1/2} 10s_{1/2})$ configuration is seen in the experimental data. The $(1s^2 2p_{1/2} 10p_{1/2})_{J=1}$ state is the only calculated state which can explain the experimental peak at 0.87 eV. The $J=0$ state of the same configuration is higher in energy, and much weaker, and does not give rise to any pronounced structure. For the $(1s^2 2p_{1/2} 10p_{3/2})$ configuration the $J=1$ and 2 states are too closely situated to be distinguishable, but the experimental peak maximum probably corresponds to the position of the stronger $J=2$ state, although the unresolved $J=1$ resonance shifts the total peak slightly to the left. There are two shoulders on the left side of the large peak, and there are only three candidates which have energy positions such that they can be responsible for these features. The $(1s^2 2p_{1/2} 10d_{3/2})_{J=2}$ state is actually the only candidate for the first shoulder. The second shoulder covers the positions of both the $J=2$ and 3 states of the $1s^2 2p_{1/2} 10d_{5/2}$ configuration. In the theoretical curve the shoulder is more structured and the peak of this structure is due to the stronger $J=3$ state. It is likely that this resonance dominates the shoulder in the experimental spectrum at 1.170 ± 0.010; see also Table IV. All states belonging to higher ℓ configurations have energy positions above 1.200 eV. They are not resolved, and build together the highest peak in the experimental data.

V. CONCLUSION

DR resonances with $\Delta n=0$ in Li-like argon have been measured with high accuracy. The absolute energies of the DR resonances were determined with a precision of $\sim 1\%$ by measuring revolution frequencies of the ions and their orbit in the ring. Further improvements to increase the accuracy are possible. Ultimately it will probably be limited by the uncertainty in the length of the beam orbit, which would give a limit of approximately 0.1%.

The splitting between the $1s^2 2p_{1/2}$ and $1s^2 2p_{3/2}$ states in Ar^{15+} was derived with an uncertainty of approximately 20 meV. This result agrees with that obtained in a more accurate astrophysical observation.

Calculations of the positions and widths of doubly excited states of Ar^{14+}, as well as of the DR rate coefficients, were performed with a method based on relativistic many-body perturbation theory. The agreement between theory and experiment is very good, and it is clear that the relativistic treatment and the inclusion of high-order correlation as well as radiative effects are crucial for the agreement.

ACKNOWLEDGMENTS

The authors would like to thank the staff of the Manne Siegbahn Laboratory for their assistance in this experiment. E.L. wants to thank A. M. Mårtensson-Pendrill for helpful discussions. This work was supported by the Swedish Natural Science Research Council (NFR) and the Knut and Alice Wallenberg Foundation.

[1] A. Burgess, Astrophys. J. **139**, 776 (1964); **141**, 1588 (1965).
[2] M. J. Seaton and P. J. Storey, in *Atomic Processes and Applications*, edited by P. G. Burke and B. L. Moisewitsch (North-Holland, Amsterdam, 1976).
[3] J. Dubau and S. Volonte, Rep. Prog. Phys. **43**, 199 (1980).
[4] H. Danared, G. Andler, L. Bagge, C. J. Herrlander, J. Hike, J. Jeansson, A. Källberg, A. Nilsson, A. Paál, K.-G. Rensfelt, U. Rosengard, J. Starker, M. af Ugglas, Phys. Rev. Lett. **72**, 3775 (1994).
[5] R. Schuch, W. Zong, D. R. DeWitt, H. Gao, S. Asp, J.

Hvarfner, E. Lindroth, H. Danared, and A. Källberg, Hyperfine Interact. **99**, 317 (1996).
[6] S. Schennach *et al.*, Z. Phys. **30**, 291 (1994).
[7] T. W. Gorczyca, F. Robicheaux, M. S. Pindzola, and N. R. Badnell, Phys. Rev. A **54**, 2107 (1996).
[8] R. Schuch, N. Badnell, D. R. DeWitt, H. Gao, S. Mannervik, W. Zong, Phys. Scr. (to be published).
[9] K. Abrahamsson *et al.*, Nucl. Instrum. Methods Phys. Res. Sect. B **79**, 269 (1993).
[10] K. Abrahamsson, G. Andler, and C. B. Bigham, Nucl. Instrum. Methods Phys. Res. Sect. B **31**, 475 (1988).
[11] D. R. DeWitt, R. Schuch, H. Gao, W. Zong, S. Asp, and C. Biedermann, Phys. Rev. A **53**, 2327 (1996).
[12] S. Asp, R. Schuch, D. R. DeWitt, C. Biedermann, H. Gao, W. Zong, D. Andler, and E. Justiniano, Nucl. Instrum. Methods Phys. Res. Sect. B **117**, 31 (1996).
[13] E. Lindroth and J. Hvarfner, Phys. Rev. A **45**, 2771 (1991).
[14] E. Lindroth, Phys. Rev. A **49**, 4473 (1994).
[15] D. R. Dewitt *et al.*, J. Phys. B **28**, L147 (1995).
[16] S. A. Blundell, Phys. Rev. A **47**, 1790 (1993).
[17] K. G. Winding and J. D. Purcell, Astrophys. J. **204**, L151 (1976).